International Journal of Precision Engineering and Manufacturing
https://doi.org/10.1007/s12541-024-01109-1
Online ISSN 2005-4602
Print ISSN 2234-7593

REGULAR PAPER

A Dual-Parallel Chamber Electromagnetic Micropump Fabricated Using 3D Printing Method from a Novel Magnetic Nanocomposite Material

Mohammad Tahmasebipour[1,2] · Shadi Ebrahimi[1,2] · Mohammad Dehghan[1,2] · Fatemeh Anousheh[1,2]

Received: 23 May 2024 / Revised: 8 August 2024 / Accepted: 9 August 2024

Abstract
Micropumps have found wide applications in biomedicine, micro-electro-mechanical systems, and microfluidic systems. This study presents a novel nozzle/diffuser micropump with two parallel chambers fabricated using the stereolithography (SLA) 3D printing method from FLGPCL04-Fe_3O_4 magnetic nanocomposite. The proposed valveless micropump is an attractive alternative for drug delivery applications due to its effective controllability, cost-effectiveness, and mass production capability. The dual chamber structure is able to overcome the disadvantages of the single chamber micropumps like providing higher flow rates. In this micropump, a maximum membrane displacement of 65 µm has been achieved using 5 wt% magnetic nanoparticles concentration for a 30-turn microcoil and applied current of 1000 mA. The fluid flow was evaluated through the membrane displacement using numerical simulations in COMSOL Multiphysics 5. Based on the experimental results, a maximum flow rate of 82 nL/s has been achieved under dual-chamber loading while loading one of the chambers leading to a maximum flow rate of 62.5 nL/s.

Keywords Micropump · Electromagnetic actuation · Nozzle/diffuser · Dual-chamber · 3D printing

1 Introduction

Based on the micro/nanofabrication technology advancements [1, 2], micro-electromechanical systems [3–9] and microfluidic systems [10, 11] have found diverse applications in advanced technologies. In the last few decades, there has been a great interest in microfluidic systems, microfluidic analysis systems, and biomedical test systems for various applications, including chemical analysis, drug delivery, diagnostic, and cell analysis [12]. Micropumps play a key role in these systems by transferring a controlled volume of fluids in different flow ranges at pL to µL. Different drive mechanisms, including piezoelectric, electromagnetic, electrostatic, electroosmotic, and pneumatic, are used to run the fluid in the micropumps [13]. In particular, electromagnetic actuators find extensive applications in various micropumps, e.g., peristaltic micropumps, where membrane actuation is carried out using electromagnetic fields. This has several advantages such as optimal power consumption, short response time, low actuation frequency, simplicity of the system, and higher membrane displacement, representing a reliable alternative in microfluidic platforms [14].

A valveless micropump consists of a membrane on the chamber and two microchannels functioning as a nozzle or diffuser, depending on the flow direction. Compared with the valved structure, the valveless structure has significant advantages such as miniaturization and anti-blocking. Also, due to the recent advances in micro-electromechanical systems (MEMS), such micropumps are widely utilized in biomedical fields. These micropumps typically have lower flow constraints in the diffuser direction; hence, a net fluid flow occurs in the diffuser direction during pumping. Moreover, nozzle/diffuser micropumps allow for outflow control. Stemme et al. (1993) introduced valveless micropump models [15] with a chamber and different diffuser designs. They used piezoelectric vibrators in their valveless micropump and obtained an optimal flow rate of 16 mL/min. Zhang et al.

✉ Mohammad Tahmasebipour
tahmasebipour@ut.ac.ir

1 Faculty of New Sciences and Technologies, University of Tehran, Tehran 14395-1561, Iran

2 Micro/Nanofabrication Technologies Lab, Faculty of New Sciences and Technologies, University of Tehran, Tehran 14395-1561, Iran

Published online: 16 August 2024

[16] reviewed piezoelectric valveless micropumps with conical channels since their wide applications in biomedicine and MEMS-based devices. Amirouche and Zhou [17] developed a valveless polydimethylsiloxane (PDMS) micropump that generated a maximum flow rate of 320 μL/min and a maximum back-pressure of 9.5 mm H2O. Zhu et al. [18] studied the effects of the diffuser angle, excitation frequency, and chamber volume on the flat piezoelectric nozzle/diffuser micropumps. Several recent studies have been conducted on magnetic nozzle/diffuser micropumps [19, 20]. Kawun et al. [21] developed a 1-mm-thick electromagnetic nozzle/diffuser micropump for biomedical applications. It generated a maximum flow rate of 135 μL/min and a maximum back-pressure of 25 mm H2O. The polymer membrane has been reported to be excited by a permanent magnet in most nozzle/diffuser micropumps to induce a repulsive/attractive mechanism. Giddle et al. [22] optimized the parameters of a valveless electromagnetic micropump. Said et al. [23] designed a valveless electromagnetic micropump with a maximum flow rate of 6.6 μL/min. Amrani et al. [24] studied a valveless electromagnetic micropump at a flow rate of 37 mL/min. Bidirectional micropumps improve system efficiency through accurate flow control. Tahmasebpour and Paknahad [25] obtained a maximum flow rate of 1.25 μL/min in a bidirectional nozzle/diffuser micropump consisting of a PDMS-Fe3O4 nanocomposite membrane. However, earlier works mostly reported single-chamber or peristaltic series micropumps, while flow measurement of dual-chamber parallel micropumps has rarely been studied. Azarbadegan et al.[26] analyzed the characteristics of a valveless dual-chamber parallel micropump using a one-dimensional nonlinear model. Chen et al. [27] investigated piezoelectric dual-chamber parallel and series micropumps. Zordan et al. [28] designed an electromagnetic dual-chamber micropump with a back pressure of 58 mm H2O. The water flow rate was maximized to 1.985 mL/s at an electric current of 1.75 A and a resonance frequency of 45 Hz. Shan et al. [29] proposed a piezoelectric valveless dual-layer chamber micropump with a small size and an adjustable flow rate. It could achieve an adjustable flow rate of 2.16–51.74 μL/min. Guo et al.[30] compared single- and dual-chamber valveless micropumps using computational modeling by the ANSYS Fluent software. Innovative methods were simultaneously developed to simplify the fabrication process of these micropumps. Several MEMS manufacturing techniques, like photolithography, are widely used to fabricate valveless micropumps. However, such methods are time-consuming and expensive, including one or more stages of accurate cleaning, adjustment, and packaging steps. Additive manufacturing is an alternative method to fabricate 2D structures from composite materials. 3D printing avoids human interactions and enables more rapid processing for complex and precise geometries. Recent advancements in the field of additive manufacturing have been presented in Ref [31].

Alam et al.[32] reported a 3D-printed miniaturized pump for microfluidic applications. Table 1 summarizes dual-chamber parallel micropumps. Several actuation mechanisms and manufacturing techniques have been studied in recent decades, depending on the application of micropumps. In this study, we developed a new 3D-printed nanocomposite micropump with a parallel dual-chamber structure. To the best of our knowledge, FLGPCL04-Fe_3O_4 3D-printed dual-chamber nozzle/diffuser micropump with parallel configuration has not been introduced, so far.

2 Principles of Operation

This study introduces a dual-chamber parallel nozzle/diffuser micropump. This nanocomposite electromagnetic micropump consists of Fe3O4 nanoparticles distributed in FLGPCL04 polymerizable optical resin. Using bulk magnets

Table 1 A summary of dual-chamber parallel micropumps

Refs.	Membrane material	Maximum flow rate	Frequency (Hz)	Fabrication method	Structure	Type
[28]	Rubber Polyisoprene membrane	1.985 ml/s	45	NA	Coaxial cantilever valve	Electromagnetic
[30]	<100> silicon	151.7 μl/min	2700	Selective-wet etching	Valveless	Piezoelectric
[27]	PMMA	32 mL/min	100	Bolts and an O-ring used to connect and seal	Umbrella type check valve	Piezoelectric
[29]	PET + PDMS	2.16–51.74 μl/min	100	Soft lithography + laser cutting	Valveless dual-layer chamber	Piezoelectric
[33]	silicon wafers ‹111›	40 <, < 60 μl/min	0.5 k	MEMS technique	Planar passive valves	Piezoelectric
[34]	Silicon	≈ 140 μl/min	20	IRE and anisotropic etching techniques	Diffuser and nozzle valve	piezoelectric
[35]	PZT + glass	60 μl/min < X < 70 μl/min	200	Wet etching	Diffuser/nozzle micro-channels	piezoelectric

increases the size of the micropump and decreases the integration capability of the micropump. Fe3O4 nanoparticles have unique properties including high magnetic properties, large surface area and low toxicity. Choosing magnetic nanopowder gave us the advantage of making a composite and reducing the size. Also, UV curable polymer FLGPCL04 is a popular clear resin with unique mechanical properties such as tensile modulus of 2.8 GPa, flexural modulus of 2.2 GPa and 6% elongation at break. The electromagnetic membrane operates when an electric current flows through the micropump coil and results in a magnetic field. This magnetic field aligns electromagnetic bipolar Fe3O4 nanoparticles, deflecting the membrane downward. Figure 1 shows a schematic form of the micropump in its pumping mode.

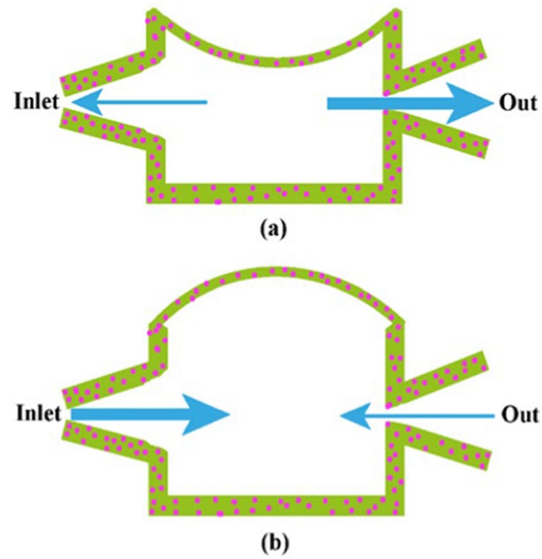

Fig. 2 Schematic form of the nanocomposite nozzle/diffuser micropump's performance: **a)** Pumping mode and **b)** supply mode

3 Design

3.1 Nozzle/Diffuser

A valveless micro-pump uses nozzle/diffuser structures to control the flow direction. Figure 2 schematically shows the working principle of the nozzle/diffuser micro-pump. A vibrating nanocomposite membrane, two nozzle/diffuser microchannels, and a fluid chamber are the valveless micropump elements. In the supplying mode, as the nanocomposite membrane actuated upward the fluid enters into the chamber due to the created negative pressure.

In contrast, during the pumping mode, the nanocomposite membrane actuates downward and causes a positive pressure inside the chamber, and then the fluid exits through the inlet and outlet channels. The design parameters of the nozzle/diffuser micro-pump are presented in Fig. 3: divergence angle (2θ), diffuser length (L), and input and output width (w1 and w2).

In nozzle/diffuser micro-pumps, the relationship between the pressure recovery coefficient and the loss coefficient is introduced by Eq. (1), when the pressure recovery coefficient increases, the loss coefficient decreases.

$$K = 1 - \left(\frac{A_{in}}{A_{out}}\right) - C_p \tag{1}$$

where C_p is the pressure recovery coefficient, K is the loss coefficient, and A_{in} and A_{out} are in the cross-section area of the entrance and the exit, respectively. The diffuser has the best performance in the transitory steady stall region where the Cp is at its maximum.

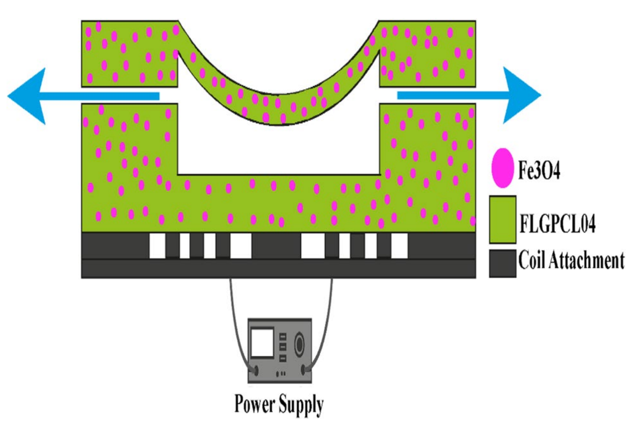

Fig. 1 Schematic form of the micropump in its pumping mode (Blue arrays display the fluid direction)

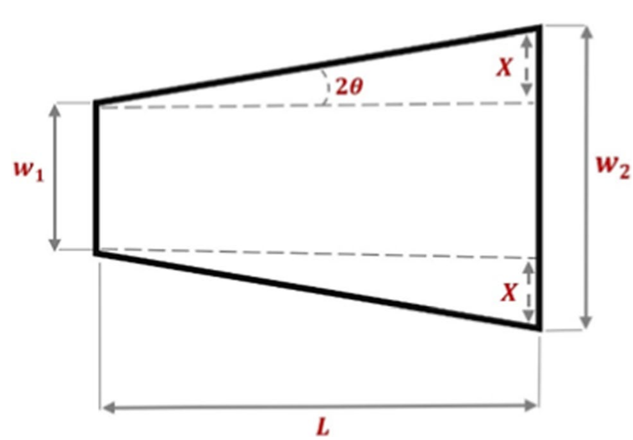

Fig. 3 The nozzle/diffuser design parameters

When 2θ is between 5–20°, l/w_1 is 16–18, and the aspect ratio is around 4, the loss coefficient K will be minimized. Other design parameters can be obtained by Eqs. (2) and (3):

$$\tan 2\theta = \frac{x}{l} \tag{2}$$

$$w_2 = w_1 + 2x \tag{3}$$

The flow rate of fluid flowing through the nozzle and diffuser can be expressed by the continuity equations of (4) and (5):

$$Q_d = A_d \times V_d \tag{4}$$

$$Q_n = A_n \times V_n \tag{5}$$

One of the major demerits of single-chamber valveless micropumps is the large vibrational pulsed flow which induces a large pressure drop, also the frictional drag losses could be significant in the connecting channels. Moreover, single-chamber pumps do not operate in a closed circuit when the fluid is incompressible. A pair of parallel chambers with out-of-phase operation could be a simple structure to cope with this challenge since the parallel pump's counter-phase movement substantially reduces the flow's larger vibrational component and physically feasible boundary conditions for a closed system with an incompressible fluid.

According to Azarbadegan et al.[26] dual-chamber parallel valveless micropumps could generate nearly twice the velocity of a dual-chamber series micropump. In this structure, the pump flow could be used in two modes, as shown in Fig. 4. In Mode 1, the total flow of two microchannels can be employed for high flow rates, while Mode 2 can be utilized for the simultaneous transfer, injection, or movement of two different fluids in a system.

Figure 5 shows the nozzle/diffuser micropump and its sizes. Table 2 reports the dimensions of the fabricated micropump.

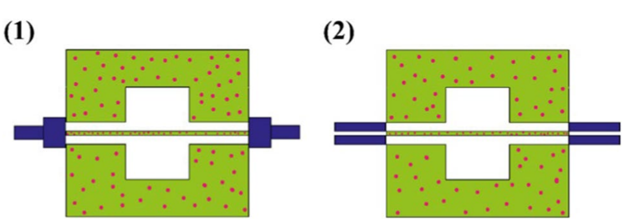

Fig. 4 Two modes for the use of dual-chamber parallel micropumps

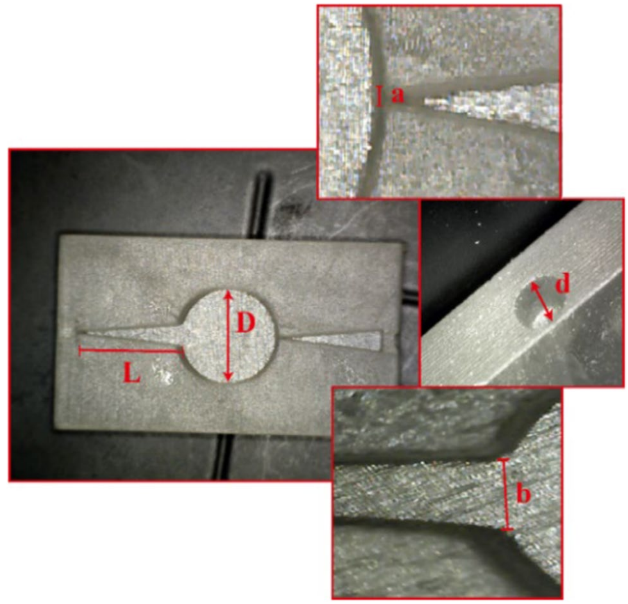

Fig. 5 Dimensional parameters of the fabricated micropump

4 Fabrication

This study introduced a 3D-printed electromagnetic dual-chamber parallel micropump. The dual parallel chambers could prevent pulsed flows and implement a steady flow. In addition, a nozzle/diffusion design was used for the channels for valveless pumping. A mixture of Fe3O4 nanoparticles and FLGPCL04 resin was homogenized using a 100 W ultrasonic homogenizer for 10 min to fabricate the micropump. The FLGPCL04-Fe_3O_4 nanoparticle mixture was then poured into the 3D printer. A Formlabs Form 3 SLA 3D printer was used to fabricate the micropump. Table 3 reports the parameters of the 3D printer. The SLA is a low-cost method with the least light diffraction and high accuracy, offering an easy and reliable workflow. Moreover, smooth and flat wall surfaces are obtained due to the uniform movement of the laser beam.

In the fabrication of the micropump using the SLA micropump, light diffraction substantially reduced since scanning is performed using a 37 µm laser beam,

Table 2 3D printed micropump geometries

Thickness	1.5 mm
Channel length(L)	5.576 mm
Channel high	800 µm
Channel width	Input(b):1200 µm Output(a):248 µm
Tube diameter(d)	1 mm
Chamber diameter(D)	5 mm

Table 3 SLA 3D printer characteristics

Laser	Light Processing Unit (LPU), 250 mW, 405 nm
Minimum Z-layer resolution	25–300 µm
XY resolution	25 µm
Connectivity	WiFi- USB
Build volume	145 × 145 × 85 mm

conveniently creating microchannels. Moreover, smooth and flat wall surfaces are obtained due to the uniform movement of the beam.

5 Micropump Characterization

Figure 6 depicts the micropump driving setup which consists of a dual-channel power supply and a switching and timing module. The flow rate measurement setup consists of a 250X digital microscope to monitor the fluid flow in the micropump outlet tube and a precise ruler with a graduation of 100 µm (0.1 mm) in length of 5 mm. Through measuring the fluid movement in a known time, the flow rate can be obtained.

A flat coil with 30 turns fabricated from the AWG30 copper wire with a minimum electrical resistance of 340 Ω was employed. A separate circuit was designed and fabricated to measure the parameters and operate the micropump. The measurement module had a magnetic sensor to measure the magnetic field, a temperature sensor, and accurate timing control. This circuit had an ATMEGA8 microcontroller as the main processor. The control circuit generates an electrical signal for the micro-coils with the capability of controlling the current, frequency, duty cycle, delay, and signal to the pattern in the micropump.

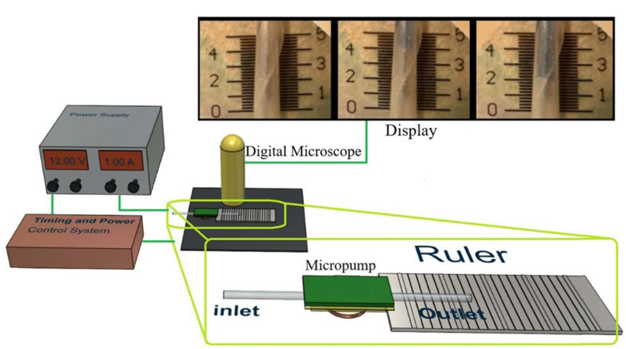

Fig. 6 The micropump characterization setup

6 Numerical Simulation

The micropump was numerically modeled in COMSOL Multiphysics 5.0. This software pack can analyze, and couple fluid flows and solid mechanics. This section briefly describes the governing equations and boundary conditions of the micropump. Using equations governing valveless micropump behavior to obtain analytical results is often difficult. Therefore, numerical simulations are efficient for predicting the behavior of such micropumps. An incompressible H_2O flow was employed, and no-slip, zero initial pressure, and suppress backflow boundary conditions were applied to the walls, inlet, and outlet, respectively. Fixed-wall conditions were also implemented on the membrane for its displacement. The membrane boundary was utilized for the fluid–structure interaction (FSI) analysis in Multiphysics. The Navier–Stokes equations of fluid flow physics were coupled with solid mechanics physics in the FSI under the aforementioned boundary conditions. The flow vectors in Fig. 7 show upward and downward membrane movements. As shown, the bottom chamber is in the pumping mode upon downward membrane movement, driving the fluid outward (Figs. 7a and b). At the same time, the top chamber is in the supply mode, driving the fluid inward. The opposite occurs when the membrane moves upward, as shown in Figs. 7c and d. These results just explain performance of the nozzle-diffuser mechanism of the micropump and determine the inlet and outlet stream lines.

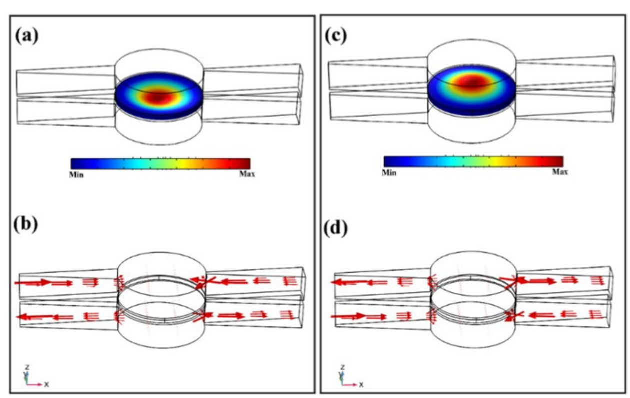

Fig. 7 Simulation results include membrane displacement contours (**a**) and (**c**), and fluid flow vectors (**b**) and (**d**) for the dual-chamber micropump

7 Results and Discussion

7.1 The Effect of Electric Current on the Magnetic Field

The effects of the current on the magnetic field created by the microcoil have been shown in Fig. 8. It can be observed that the magnetic field magnitude increases with increasing the electric current. A magnetic field of 34 mT is obtained for a 30-turn coil at the top center of the coil for a current of 1000 mA. Therefore a coil with 30 turns and an electric current of 1000 mA has been selected for the other tests since fewer turns would require a larger magnetic field to actuate the electromagnetic micropump.

7.2 The Effect of the Fe3O4 Nanoparticles on Membrane Displacement

Five magnetic membranes and five Fe_3O_4 nanoparticle fractions were tested to implement membrane deflections. Increasing the nanoparticles concentration up to 5 wt% was found to raise the membrane deflection. However, a further increase in the Fe_3O_4 nanoparticles concentration higher than 5 wt% reduced the nanocomposite membrane deflection due to lower membrane flexibility.

As mentioned before, the coil with 30 turns and 1000 mA current was used to actuate the membranes. Figure 9 plots the membrane deflection versus actuation time with 5 wt% nanoparticles concentration. The membrane experienced a maximum deflection of 65 µm for an electric current of 1000 mA in 12 s.

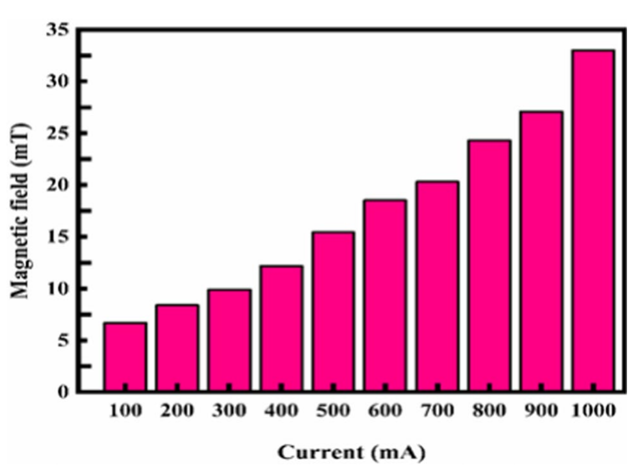

Fig. 8 Magnetic field versus electric current

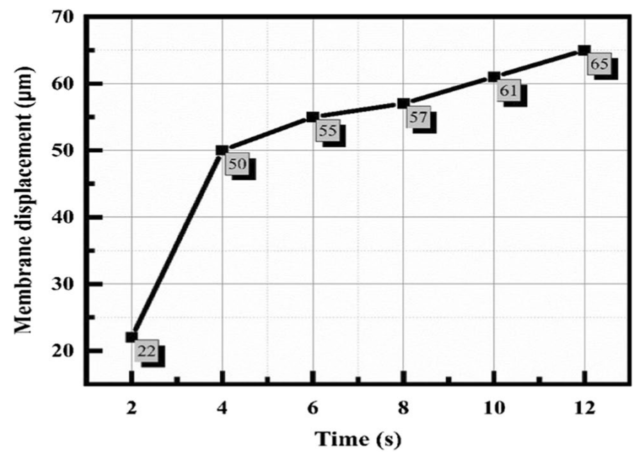

Fig. 9 Membrane displacement as a function of time for 5 wt% nanoparticles concentration

7.3 Fluid Flow in the 3D-Printed Micropump

Figure 10 shows the fluid flow rate of the micropump versus the period. Two scenarios were assumed to evaluate the flow rate in the printed micropump: (1) Both chambers contained fluids and (2) only the bottom chamber contained fluid. Signals with periods of 4, 8, 12, 16, 20, and 24 s were applied to the micropumps. The membrane was bidirectionally deflected by two parallel coils to displace the membrane in positive and negative directions. The flow rate was maximized to 62.5 nL/s in 8 s (4 s suction, 4 s compression) when only one chamber was loaded and to 82 nL/s in 16 s for dual chambers (8 s suction, 8 s compression). A rise in the oscillation of electrical pulses applied to the micropump to further deflect the membrane reduced the pumping frequency, reducing the flow rate. There is no sufficient time for membrane deflection at intervals shorter than 8–16 s, leading to lower flow rates.

Furthermore, the duty cycle changes influence the flow rate. As shown in Fig. 11, the duty cycle was 60 and 50%

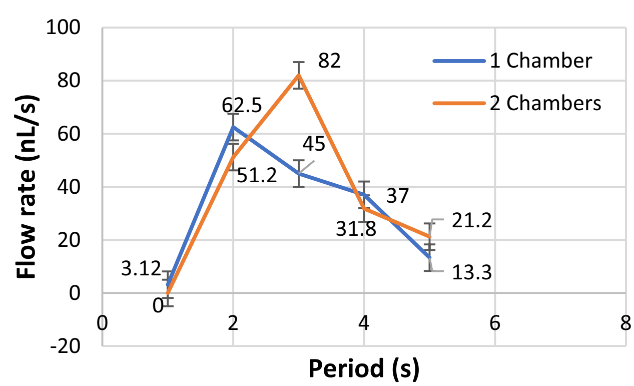

Fig. 10 Fluid flow rate versus the period

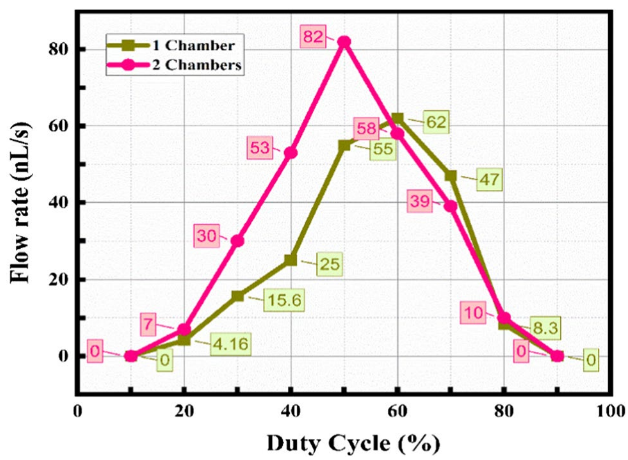

Fig. 11 Fluid flow rate versus the duty cycle

at 8 and 16 s, respectively. An increase or decrease in the duty cycle decreases the flow velocity. Thus, flow rate control using the duty cycle is a characteristic of the proposed micropump, determining the positive and negative deflections of the membrane during a cycle. An increase in the duty cycle lengthened membrane tension (into the chamber) over a cycle; hence, the membrane applies a greater force to the fluid, increasing the pumping rate. Moreover, membrane restoration is decelerated, and the membrane undergoes a smaller deflection in the next cycle, leading to insufficient time for the inward flow of the fluid. The proposed micropump allows for effectively controlling the flow rate using the duty cycle.

Micropumps with similar flow rates are used for transporting fluid in the micro-total analysis system (Micro-TAS), point of care testing (POCT) systems and lab-on-a-chip (LOC) systems. A similar micropump with the flow rate of 27.78 nL/s has been used for an implantable drug delivery system [36].

8 Conclusion

This study introduced an electromagnetic nanocomposite dual-chamber parallel micropump. Straightforward, rapid manufacturing using an SLA 3D printer was employed. The characterization of the micropump indicated that the membrane deflection was 65 µm at a Fe3O4 nanoparticle mass fraction of 5%, a current of 1000 mA, and a 30 coil turn. Dual-chamber loading maximized the flow rate to 82 nL/s at a period of 16 s, which was larger than the maximum flow rate in the single-chamber loading scenario. The proposed micropump can be employed in two operating modes to inject or transfer two different fluids or one fluid to increase the flow rate within microfluidic systems further.

References

1. Tahmasebipour, M., Tahmasebipour, Y., & Vafaie, A. (2019). Micro wire electrical discharge machining of MEMS structures with optimized dimensional deviation. *ADMT Journal, 12*(2), 103–109.
2. Tahmasebipour, G., Tahmasebipour, Y., & Ghoreishi, M. (2011). Computational fluid dynamic simulation of the nano-electrical discharge machining process. *NANO, 6*(06), 561–568.
3. Tahmasebipour, M., & Vafaie, A. (2017). A highly sensitive three axis piezoelectric microaccelerometer for high bandwidth applications. *Micro and Nanosystems, 9*(2), 111–120. https://doi.org/10.2174/1876402910666180118124845
4. Tahmasebipour, M., & Modarres, M. (2018). Simulation of a Highly Sensitive Piezoresistive Differential Pressure Microsensor. *Iranian Journal of Electrical and Electronic Engineering, 14*(4), 374–381.
5. Tahmasebipour, M., & Sangchap, M. (2019). A novel high performance integrated two-axis inchworm piezoelectric motor. *Smart Materials and Structures., 29*(1), 015034. https://doi.org/10.1088/1361665X/ab545e
6. Vafaie, A., Tahmasebipour, M., & Tahmasebipour, Y. (2019). A novel capacitive micro-accelerometer made of steel using micro wire electrical discharge machining method. *Journal of Micromechanics and Microengineering, 29*(12), 125018. https://doi.org/10.1088/1361-6439/ab
7. Sangchap, M., Tahmasebipour, M., & Tahmasebipour, Y. (2020). A linear Inchworm Piezomotor with a new configuration: design considerations, fabrication and characterization. *Iranian Journal of Science and Technology, Transactions of Mechanical Engineering., 16*, 1–2.
8. Tahmasebipour, M., & Vafaie, A. (2020). A novel single axis capacitive MEMS accelerometer with double-sided suspension beams fabricated using µWEDM. *Sensors and Actuators A: Physical*. https://doi.org/10.1016/j.sna.2020.112003
9. Gwon, M., Park, G., Hong, D., Park, Y. J., Han, S., Kang, D., & Koh, J. S. (2022). Soft directional adhesion gripper fabricated by 3D printing process for gripping flexible printed circuit boards. *International Journal of Precision Engineering and Manufacturing-Green Technology, 9*(4), 1151–1163. https://doi.org/10.1007/s40684-021-00368-x
10. Paknahad, A. A., & Tahmasebipour, M. (2019). An electromagnetic micro-actuator with PDMS-Fe_3O_4 nanocomposite magnetic membrane. *Microelectronic Engineering, 5*, 111031. https://doi.org/10.1016/j.mee.2019.111031
11. Ebrahimi, S., & Tahmasebipour, M. (2022). Numerical study of a centrifugal platform for the inertial separation of circulating tumor cells using contraction-expansion array microchannels. *Archives of Razi Institute, 77*(2), 647–660.
12. Au, A. K., et al. (2011). Microvalves and micropumps for BioMEMS. *Micromachines, 2*(2), 179–220.
13. Tahmasebipour, M., & Dehghan, M. (2022). A novel electromagnetic microactuator with a stainless steel mas-spring structure. *Journal of Micromechanics and Microengineering, 32*(12), 125001.
14. Sakamoto, R., et al. (2008) Design and fabrication process of a micropump using bulk Pb (Zr, Ti) O3 for microfluidic devices. In: *Device and Process Technologies for Microelectronics, MEMS, Photonics, and Nanotechnology* IV. SPIE.
15. Stemme, E., & Stemme, G. (1993). A valveless diffuser/nozzle-based fluid pump. *Sensors and Actuators A: Physical, 39*(2), 159–167.
16. Zhang, B.-c. et al. (2017) Design and research on the piezoelectric pump of single—Cavity dual—Outlet with bluff bodies.

In: 2017 Symposium on Piezoelectricity, Acoustic Waves, and Device Applications (SPAWDA). IEEE.
17. Zhou, Y., & Amirouche, F. (2011). An electromagnetically-actuated all-PDMS valveless micropump for drug delivery. *Micromachines, 2*(3), 345–355.
18. He, X., et al. (2017). The analysis of internal transient flow and the performance of valveless piezoelectric micropumps with planar diffuser/nozzles elements. *Microsystem Technologies, 23*, 23–37.
19. Ruslia, M. A., Chee, P. S., & Leow, P. L. (2017). Characterization of electromagnetic valveless micropump. *TELKOMNIKA (Telecommunication Computing Electronics and Control), 15*(2), 771–777.
20. Mi, S., et al., A minimized valveless electromagnetic micropump for microfluidic actuation on organ chips. *sensors and actuators A: Physical*, 2020. 301: p. 111704.
21. Kawun, P., Leahy, S., & Lai, Y. (2016). A thin PDMS nozzle/diffuser micropump for biomedical applications. *Sensors and Actuators A: Physical, 249*, 149–154.
22. Gidde, R. R., et al. (2019). Design optimization of an electromagnetic actuation based valveless micropump for drug delivery application. *Microsystem Technologies, 25*, 509–519.
23. Said, M. M., et al. (2017). Hybrid polymer composite membrane for an electromagnetic (EM) valveless micropump. *Journal of Micromechanics and Microengineering, 27*(7), 075027.
24. Amrani, I., Cheriet, A., & Feliachi, M. (2018). Design and experimental investigation of a bi-directional valveless electromagnetic micro-pump. *Sensors and Actuators A: Physical, 272*, 310–317.
25. Tahmasebipour, M., & Paknahad, A. A. (2019). Unidirectional and bidirectional valveless electromagnetic micropump with PDMS-Fe3O4 nanocomposite magnetic membrane. *Journal of Micromechanics and Microengineering, 29*(7), 075014.
26. Azarbadegan, A., et al. (2010). Analysis of dual-chamber parallel valveless micropumps. *Microfluidics and Nanofluidics, 9*, 171–180.
27. Chen, S., et al. (2019). A dual-chamber serial–parallel piezoelectric pump with an integrated sensor for flow rate measurement. *Sensors, 19*(6), 1447.
28. Zordan, E., Amirouche, F., & Zhou, Y. (2010). Principle design and actuation of a dual chamber electromagnetic micropump with coaxial cantilever valves. *Biomedical microdevices, 12*, 55–62.
29. Shan, J., et al. (2022). Implantable dual-layer pump chamber piezoelectric valveless micropump with adjustable flow rate function. *Journal of Micromechanics and Microengineering, 32*(10), 105002.
30. Guo, L., et al. (2012). Valveless piezoelectric micropump of parallel dual chambers. *International Journal of precision engineering and manufacturing, 13*, 771–776.
31. Rosen, D. W. (2024). The Current Design for Additive Manufacturing Research Frontier. *International Journal of Precision Engineering and Manufacturing-Smart Technology, 2*(1), 1–4.
32. Alam, M. N. H. Z., et al. (2017). Design and fabrication of a 3D printed miniature pump for integrated microfluidic applications. *International Journal of Precision Engineering and Manufacturing, 18*, 1287–1296.
33. Hsu, C.-J., & Sheen, H.-J. (2009). A microfluidic flow-converter based on a dual-chamber planar micropump. *Microfluidics and nanofluidics, 6*, 669–678.
34. Guu, Y., Hocheng, H., & Chang, C. (2008). Study of piezoelectrically actuated micropumps with multiple parallel chambers. *Materials and Manufacturing Processes, 23*(2), 209–214.
35. Guan, Y., et al. (2020). Experimental investigation of piezoelectric micropumps with single, series or parallel pump chambers. *International Journal of Acoustics and Vibration, 25*(3), 453–460.
36. Maillefer, Disier, et al. A high-performance silicon micropump for an implantable drug delivery system. Technical Digest. IEEE International MEMS 99 Conference. Twelfth IEEE International Conference on Micro Electro Mechanical Systems (Cat. No. 99CH36291).

Mohammad Tahmasebipour is an associate professor in the Faculty of New Sciences and Technologies at the University of Tehran (Iran).

His research interests include Nanotechnology, MEMS/NEMS, Micro/Nanofluidic Systems, Micro/Nano Sensors & Actuators, Nanophotonics, Micro/Nano-Fabrication Technologies, Nanomaterials, Nanocomposites, Flexible Sensors and Actuators, Wearable Sensors and Systems, Flexible Solar Cells, Flexible Energy Harvesters, Wearable Technologies, and Optical Fiber Sensors and Systems. Dr. M. Tahmasebipour is a recipient of the World Academy of Sciences (TWAS) prize to young scientists, 24th Khwarizmi International Award from the President of Iran, The Research and Innovation Award from the Iran's National Elites Foundation, and the gold medal from the ECO Cultural Institute.

Shadi Ebrahimi received the B.E. degree in mechanical engineering from the Tabriz University, Tabriz, Iran and the M.S degrees in MEMS & NEMS engineering from the Faculty of New Sciences and Technologies, University of Tehran, Tehran, Iran. His current research interests include MEMS and Microfluidic systems.

Mohammad Dehghan received the B.E. degree in electrical engineering from the Azad University of Science and Research (Fars), Shiraz, in 2014, and the M.S degrees in MEMS & NEMS engineering from the Faculty of New Sciences and Technologies, University of Tehran, Tehran, Iran, in 2017. His current research interests include MEMS inertial sensors, Microfluidic systems, and design and implementation of electronic circuits used in microsystems.

Fatemeh Anousheh received the B.E. degree in engineering science from the University of Tehran and she is M.S student in MEMS & NEMS engineering at the Faculty of New Sciences and Technologies, University of Tehran, Tehran, Iran. His current research interests include MEMS and Microfluidic systems.